



(<https://www.elsevier.com>)

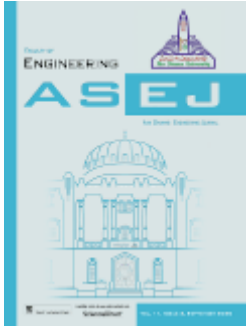
ELSEVIER  
ELSEVIER

SEARCH

MENU

Home (<https://www.elsevier.com/>) > Journals (<https://www.elsevier.com/catalog?producttype...>)

> Ain Shams Engineering Journal (<https://www.journals.elsevier.com:443/ain-shams-engineering-journal>)



(<https://www.sciencedirect.com/science/journal/20904479>)

ISSN: 2090-4479

# Ain Shams Engineering Journal

Chief Editorial Board: Professor Ayman M. Bahaa-Eldin

(<https://www.journals.elsevier.com:443/ain-shams-engineering-journal/editorial-board/professor-ayman-m-bahaa-eldin>), Professor Diaa Khalil

(<https://www.journals.elsevier.com:443/ain-shams-engineering-journal/editorial-board/professor-diaa-khalil>)

> View Editorial Board (<https://www.journals.elsevier.com:443/ain-shams-engineering-journal/editorial-board>)

> CiteScore: 4.6 ⓘ Impact Factor: 1.949 ⓘ

Submit Your Paper



Open Access (<https://www.elsevier.com/journals/ain-shams-engineering-journal/2090-4479/open-access-journal>)

View Articles (<https://www.sciencedirect.com/science/journal/20904479>)

(/ain (http  
- s://w  
sha ww.e  
ms- lsevi  
engi er.co  
neeri m/Pr  
ng- efere  
jour nceC  
nal/r entre  
ss) )

## Track Your Paper

*Ain Shams Engineering Journal* is an international journal devoted to publication of peer reviewed original high-quality research papers and review papers in both traditional topics and those of emerging science and technology. Areas of both theoretical and fundamental interest as well as those concerning...

Read more

## Journal Metrics

> CiteScore: **4.6** ⓘ

Impact Factor: **1.949** ⓘ

Source Normalized Impact per Paper (SNIP): **1.212** ⓘ

SCImago Journal Rank (SJR): **0.402** ⓘ

> View More on Journal Insights

## Your Research Data

> Share your research data (<https://www.elsevier.com/authors/author-resources/research-data>)

## Society Links



أكاديمية البحث  
العلمي والتكنولوجيا  
Academy of Scientific  
Research & Technology

(<http://www.asrt.sci.eg>)

## Related Links

> Author Stats ⓘ

> Researcher Academy

> Author Resources (<https://www.elsevier.com/authors/author-resources>)

> Try out personalized alert features



(<https://www.elsevier.com>)

ELSEVIER  
ELSEVIER



SEARCH



MENU

Production and Hosting by Elsevier B.V. on behalf of Ain Shams University  
Peer Review under the responsibility of Ain Shams University

Most Downloaded   Recent Articles   Most Cited

Sentiment analysis algorithms and applications: A survey - Open access

Wala Medhat | Ahmed Hassan | ...

Managing risks of the Grand Ethiopian Renaissance Dam on Egypt - Open access

Wala Y. El-Nashar | Ahmed H. Elyamany

Enhancing the performance of photovoltaic panels by water cooling - Open access

K.A. Moharram | M.S. Abd-Elhady | ...

[View All Most Downloaded Articles \(https://www.journals.elsevier.com:443/ain-shams-engineering-journal/most-downloaded-articles\)](https://www.journals.elsevier.com:443/ain-shams-engineering-journal/most-downloaded-articles)

Most Downloaded Articles



Recent Articles



Most Cited Articles



(/ain (http  
- s://w  
sha ww.e  
ms- lsevi  
engi er.co  
neeri m/Pr  
na ofere



Elsevier stands against racism and discrimination and fully supports the joint commitment for action in inclusion and diversity in publishing.

In partnership with the communities we serve; we redouble our deep commitment to inclusion and diversity within our editorial, author and reviewer networks.

Visibility. Trust. Choice. Only some of the benefits of publishing open access with Elsevier (https://www.journals.elsevier.com:443/ain-shams-engineering-journal/announcements/visibility-trust-choice-only-some-of-the-benefits-of-publish)

Discover how our open access options can help you maximize reach and impact

> View All (https://www.journals.elsevier.com:443/ain-shams-engineering-journal/announcements)

### PlumX Metrics (https://www.journals.elsevier.com:443/ain-shams-engineering-journal/top-articles)

Below is a recent list of 2019—2020 articles that have had the most social media attention. The Plum Print next to each article shows the relative activity in each of these categories of metrics: Captures, Mentions, Social Media and Citations. Go here to learn more about PlumX Metrics.



Nature-inspired algorithms for feed-forward neural network classifiers: A survey of one decade of research

(https://pl

u.mx/a?doi=10.1016/j.asej.2020.01.001

The effects of mainshock-aftershock in successive earthquakes on the response of RC moment-resisting frames considering the influence of the vertical seismic component

(https://doi.org/10.1016/j.asej.2020.01.001)

Vertical gardens as a restorative tool in urban spaces of New Cairo

(https://doi.org/10.1016/j.asej.2020.01.001)

(https://pl

u.mx/a?doi=10.1016/j.asej.2020.01.001

(https://pl

u.mx/a?doi=10.1016/j.asej.2020.01.001

News (https://www.journals.elsevier.com:443/ain-shams-engineering-journal/news)

(https://pl

u.mx/a?doi=10.1016/j.asej.2020.01.001

[View All \(https://www.journals.elsevier.com:443/ain-shams-engineering-journal/news\)](https://www.journals.elsevier.com:443/ain-shams-engineering-journal/news)

[ide Usage \(https://www.elsevier.com\)](https://www.elsevier.com)

 **SEARCH**  **MENU**

# Ain Shams Engineering Journal

---

Readers

[View Articles](#)

[Volume/ Issue Alert](#)

[Personalized Recommendations](#)

[User rights \(https://www.elsevier.com/journals/ain-shams-engineering-journal/2090-4479/user-rights\)](https://www.elsevier.com/journals/ain-shams-engineering-journal/2090-4479/user-rights)

[Authors \(http://www.elsevier.com/authors/home\)](http://www.elsevier.com/authors/home)

[Author Information Pack \(https://www.elsevier.com/journals/ain-shams-engineering-journal/2090-4479?generatepdf=true\)](https://www.elsevier.com/journals/ain-shams-engineering-journal/2090-4479?generatepdf=true)

[Submit Your Paper](#)

[Track Your Paper](#)

[Researcher Academy](#)

[Rights and Permissions \(https://www.elsevier.com/about/policies/copyright/permissions\)](https://www.elsevier.com/about/policies/copyright/permissions)

[Elsevier Author Services](#)

[Support Center](#)

[Librarians \(https://www.elsevier.com/librarians\)](https://www.elsevier.com/librarians)

[Abstracting/ Indexing \(http://www.elsevier.com/journals/ain-shams-engineering-journal/2090-4479/abstracting-indexing\)](http://www.elsevier.com/journals/ain-shams-engineering-journal/2090-4479/abstracting-indexing)

[Editors \(http://www.elsevier.com/editors/home\)](http://www.elsevier.com/editors/home)

[Publishing Ethics Resource Kit \(http://www.elsevier.com/editors/perk\)](http://www.elsevier.com/editors/perk)

[Support Center](#)

[Reviewers \(http://www.elsevier.com/reviewers/home\)](http://www.elsevier.com/reviewers/home)

[Log in as Reviewer](#)

[Reviewer Recognition \(https://www.elsevier.com/reviewers/becoming-a-reviewer-how-and-why#recognizing\)](https://www.elsevier.com/reviewers/becoming-a-reviewer-how-and-why#recognizing)

[Support Center](#)

[Societies \(http://www.elsevier.com/societies/home\)](http://www.elsevier.com/societies/home)



[\(https://www.elsevier.com\)](https://www.elsevier.com)

**ELSEVIER**

Copyright © 2020 Elsevier B.V.

[Careers \(https://www.elsevier.com/careers/careers-with-us\)](https://www.elsevier.com/careers/careers-with-us) - [Terms and Conditions](#)

[\(https://www.elsevier.com/legal/elsevier-website-terms-and-conditions\)](https://www.elsevier.com/legal/elsevier-website-terms-and-conditions) - [Privacy Policy](#)

[\(https://www.elsevier.com/legal/privacy-policy\)](https://www.elsevier.com/legal/privacy-policy)

Cookies are used by this site. To decline or learn more, visit our [Cookies page](#).



(<https://www.elsevier.com>)

 RELX Group™ (<http://www.reedelsevier.com/>)



SEARCH



MENU

ELSEVIER  
ELSEVIER  
ELSEVIER

ww.elsevi  
er.com)



(<https://www.mendeley.com/groups/>)

 RELX Group™ (<http://www.reedelsevier.com/>)

(<https://twitter.com/ElsevierCon>)  
(<https://www.facebook.com/ElsevierCompany>)  
(<https://www.linkedin.com/company/elsevier>)  
nnect) reed-elsevier)



ScienceDirect

# Ain Shams Engineering Journal

| *Open access*

Latest issue   All issues   ●●●

---

[Search in this journal](#)

---

## About the journal

[Aims and scope](#)   [Editorial board](#)   [Abstracting and indexing](#)

---

*Ain Shams Engineering Journal* is an international journal devoted to publication of peer reviewed original high-quality research papers and review papers in both traditional topics and those of emerging science and technology. Areas of both theoretical and fundamental interest as well as those concerning industrial applications, emerging instrumental techniques and those which have some practical application to an aspect of human endeavor, such as the preservation of the environment, health, waste disposal are welcome. The overall focus is on original and rigorous scientific research results which have generic significance.

*Ain Shams Engineering Journal* focuses upon aspects of mechanical engineering, electrical engineering, civil engineering, chemical engineering, petroleum engineering, environmental engineering, architectural and urban planning engineering. Papers in which knowledge from other disciplines is integrated with engineering are especially welcome like nanotechnology, material sciences, and computational methods as well as applied basic sciences: engineering mathematics, physics and chemistry.

For queries related to the journal, please contact [editor@eng.asu.edu.eg](mailto:editor@eng.asu.edu.eg)

---

ISSN: 2090-4479



[About ScienceDirect](#)

[Remote access](#)

[Shopping cart](#)

[Advertise](#)

[Contact and support](#)

[Terms and conditions](#)

[Privacy policy](#)

We use cookies to help provide and enhance our service and tailor content and ads. By continuing you agree to the **use of cookies**.

Copyright © 2020 Elsevier B.V. or its licensors or contributors. ScienceDirect® is a registered trademark of Elsevier B.V.

ScienceDirect® is a registered trademark of Elsevier B.V.



# Ain Shams Engineering Journal

## CHIEF EDITORIAL BOARD

Prof. Ayman M. Bahaa-Eldin  
Fac. of Engineering, Ain Shams University,  
Cairo, Egypt  
E-mail: ayman.bahaa@eng.asu.edu.eg

Prof. Diaa Khalil  
Fac. of Engineering, Ain Shams University,  
Cairo, Egypt  
E-mail: diaa\_khalil@eng.asu.edu.eg

## EDITORIAL BOARD

Prof. Morad Abdel-Kader  
Fac. of Engineering, Ain Shams University,  
Cairo, Egypt  
E-mail: moradabdelkader@gmail.com

Dr. Mohamed Abdelaziz  
Fac. of Engineering, Ain Shams University,  
Cairo, Egypt  
E-mail: mohamed\_abdelaziz@eng.asu.edu.eg

Dr. Hossam Eldin Hassan Abdelmunim  
Fac. of Engineering, Ain Shams University,  
Cairo, Egypt  
E-mail: hossameldin.hassan@eng.asu.edu.eg

Prof. Nahla AboulAtta  
Fac. of Engineering, Ain Shams University,  
Cairo, Egypt  
E-mail: nahla\_abdelhamid@eng.asu.edu.eg

Prof. Sohair Imam Abou-Elela  
National Research Center, Giza, Egypt  
E-mail: sohairela@gmail.com

Dr. Ghada Bassioni  
Fac. of Engineering, Ain Shams University,  
Cairo, Egypt  
E-mail: ghada\_bassioni@eng.asu.edu.eg

Prof. Alaa Chateauf  
Université Blaise Pascal, Aubière, France  
E-mail: alaa.chateauf@univ-bpclermont.fr

Prof. Mina Dawood  
Cullen College of Engineering,  
University of Houston, USA  
E-mail: mmdawood@uh.edu

Dr. Rabab Moustafa Ibrahim El-Hassani  
Fac. of Engineering, Ain Shams University,  
Cairo, Egypt  
E-mail: rabab\_elhassani@eng.asu.edu.eg

Prof. Fathalla Mohamed Fathalla El-Nahhas  
Fac. of Engineering, Ain Shams University,  
Cairo, Egypt  
E-mail: fathalla\_elnahhas@eng.asu.edu.eg

Dr. Abeer Elshater  
Fac. of Engineering, Ain Shams University,  
Cairo, Egypt  
E-mail: abeer.elshater@eng.asu.edu.eg

Prof. Amir Fam  
Fac. of Engineering and Applied Science,  
Queen's University, Kingston, Canada  
E-mail: fam@civil.queensu.ca

Prof. Hany Hasani  
Fac. of Engineering, Ain Shams University,  
Cairo, Egypt  
E-mail: hany\_mohamed@eng.asu.edu.eg

Prof. Sameh Ibrahim  
Fac. of Engineering, Ain Shams University,  
Cairo, Egypt  
E-mail: sameh.ibrahim@eng.asu.edu.eg

Prof. Mohamad Y. Jaber  
Dept. of Mechanical and Industrial  
Engineering, Ryerson University,  
Toronto, Canada  
E-mail: mjaber@ryerson.ca

Prof. Shelly Lissel  
Schulich School of Engineering,  
University of Calgary, Calgary, Canada  
E-mail: slissel@ucalgary.ca

Dr. Ehab Mina  
Fac. of Engineering, Ain Shams University,  
Cairo, Egypt  
E-mail: ehab\_mina@eng.asu.edu.eg

Prof. Tarek Kamal Hassan Mohamed  
Fac. of Engineering, Ain Shams University,  
Cairo, Egypt  
E-mail: tarek\_kamal@eng.asu.edu.eg

Dr. Fatma Newagy  
Fac. of Engineering, Ain Shams University,  
Cairo, Egypt  
E-mail: fatma\_newagy@eng.asu.edu.eg

Prof. Heinz Palkowski  
Inst. of metallurgy,  
Clausthal University of Technology,  
Clausthal-Zellerfeld, Germany  
E-mail: heinz.palkowski@tu-clausthal.de

Dr. Yasser Mohammed Sabry  
Fac. of Engineering, Ain Shams University,  
Cairo, Egypt  
E-mail: yasser.sabry@eng.asu.edu.eg

Prof. Amr Shaat  
Fac. of Engineering, Ain Shams University,  
Cairo, Egypt  
E-mail: amr.shaat@eng.asu.edu.eg

Dr. Rania Swief  
Fac. of Engineering, Ain Shams University,  
Cairo, Egypt  
E-mail: Rania.Abel-Wahed@eng.asu.edu.eg

Prof. Dirk Turschner  
Inst. of Electrical Power Engineering and  
Energy Systems, Clausthal University  
of Technology, Clausthal, Germany  
E-mail: dirk.turschner@tu-clausthal.com

Prof. Ahmaed Hassan Yousuf  
Fac. of Engineering, Ain Shams University,  
Cairo, Egypt  
E-mail: ahassan@eng.asu.edu.eg

Prof. Gerhaard Ziegmann  
Inst. of Polymer Materials and Plastics  
Engineering, Clausthal University of Technology,  
Clausthal, Germany  
E-mail: Ziegmann@puk.tu-clausthal.de

## EDITORIAL TECHNICAL OFFICE

Dr. Ahmed Sami Abd Elrahman  
Fac. of Engineering, Ain Shams University,  
Cairo, Egypt  
E-mail: ahmed.sami@eng.asu.edu.eg

Mrs. Rayda Ahmed  
Fac. of Engineering, Ain Shams University,  
Cairo, Egypt  
E-mail: asej.rayda@gmail.com

Dr. Mohamed ElFayoumi  
Fac. of Engineering, Ain Shams University,  
Cairo, Egypt  
E-mail: m\_fayoumi@eng.asu.edu.eg

Dr. Mohamed Kohail  
Fac. of Engineering, Ain Shams University,  
Cairo, Egypt  
E-mail: m.kohail@eng.asu.edu.eg



ScienceDirect

# Ain Shams Engineering Journal

| *Open access*

[Latest issue](#)

[All issues](#)



---

[Search in this journal](#)

---

## About the journal

[Aims and scope](#)

[Editorial board](#)

[Abstracting and indexing](#)

---

Directory of Open Access Journals (DOAJ)

Ei Compendex

Emerging Sources Citation Index (ESCI)

INSPEC

Science Citation Index Expanded

Scopus

---

ISSN: 2090-4479

Copyright © 2020 Ain Shams University. Production and hosting by Elsevier B.V. All rights reserved

---



[About ScienceDirect](#)

[Remote access](#)

[Shopping cart](#)

[Advertise](#)

[Contact and support](#)

[Terms and conditions](#)

[Privacy policy](#)

We use cookies to help provide and enhance our service and tailor content and ads. By continuing you agree to the **use of cookies**.

Copyright © 2020 Elsevier B.V. or its licensors or contributors. ScienceDirect® is a registered trademark of Elsevier B.V.

ScienceDirect® is a registered trademark of Elsevier B.V.





Contents lists available at ScienceDirect

Ain Shams Engineering Journal

journal homepage: www.sciencedirect.com



Civil Engineering

## Integrated time-frequency wavelet analysis and impulse response filtering on SASW test for rigid pavement stiffness prediction

Sri Atmaja P. Rosyidi<sup>a</sup>, Nur Izzi Md. Yusoff<sup>b,\*</sup>, Norfarah Nadia Ismail<sup>c</sup>, Muhamad Razuhanafi Mat Yazid<sup>b</sup><sup>a</sup> Dept. of Civil Engineering, Universitas Muhammadiyah Yogyakarta, Jalan Brawijaya (Lingkar Selatan), Bantul, 55183 Yogyakarta, Indonesia<sup>b</sup> Dept. of Civil Engineering, Universiti Kebangsaan Malaysia, 43600 Bangi, Selangor, Malaysia<sup>c</sup> Dept. of Civil Engineering, International Islamic University Malaysia, Gombak, Selangor, Malaysia

## ARTICLE INFO

## Article history:

Received 29 January 2020

Accepted 13 May 2020

Available online xxx

## Keywords:

Pavement stiffness

PCC rigid pavement

Surface wave technique

## ABSTRACT

This paper employs an improved continuous wavelet transform (CWT) technique of Gaussian derivative function and impulse response filtering (IRF) in seismic surface wave analysis to improve data analysis in the Spectral Analysis of Surface Wave (SASW) method. Two procedures were used: first, the response spectrum of interest was chosen using a time–frequency wavelet spectrogram. Then, noisy distortions were eliminated by utilizing a time–frequency wavelet and impulse response filtering. The outcomes show that the SASW method is able to identify the surface wave velocity which coincides with the dynamic stiffness parameters of Portland Cement Concrete (PCC) slabs. The values of surface wave velocity increased during the curing stage, and in situ measurement of wave velocity could be helpful in determining the degree of curing. A good congruence has been demonstrated between the stiffness of PCC obtained from SASW measurements vis a vis that obtained using the American Concrete Institute (ACI) formulation.

© 2020 THE AUTHORS. Published by Elsevier BV on behalf of Faculty of Engineering, Ain Shams University. This is an open access article under the CC BY-NC-ND license (<http://creativecommons.org/licenses/by-nc-nd/4.0/>).

## 1. Introduction

The stiffness and thickness of Portland cement concrete (PCC) slabs of rigid pavement structures are two important parameters in construction. In most cases, pavement stiffness must be established prior to designing, monitoring, and evaluating highway pavements. Conventional tests, such as field coring and laboratory compressive strength, are usually carried out to determine these parameters. Coring tests are time consuming and are only carried out occasionally. For this reason, the most critical segments of pavement structure in terms of stiffness (strength) and thickness are sometimes ignored and not tested. To deal with this problem,

it is crucial to find a quick and efficient method for determining the stiffness and thickness of PCC slabs.

A non-destructive (NDT) method known as Spectral Analysis of Surface Wave (SASW) has been established on the Rayleigh ( $R$ ) wave propagation; it was designed to establish shear wave velocity in relation to material stiffness and the depth of individual layer of pavement profile. Contrary to the Impact Echo and Ultrasonic Pulse Velocity methods which are dependent on the measured wave velocities and are employed to evaluate thickness and identify flaw, the SASW method provides the details on the variation of material properties with depth by using wave dispersion [1]. SASW operates entirely on the surface of rigid pavement profiles without physically intruding into the structures. This method is an improvement made by Nazarian and Stokoe [2] on the frequently employed steady-state technique developed by Jones [3]. Since the last decade the SASW method has been used in different applications. These applications include characterization of foundations; determination of soil profile; concrete structure assessment; identification of ground anomalies, such as soil lenses and dipping layers; identification of the structural layer of cement mortar; assessment of compaction on fill structure; and assessment of railway ballast. The SASW method was first used on concrete by Nazarian and Stokoe [4] and the results of their study

\* Corresponding author.

E-mail addresses: [atmaja\\_sri@umy.ac.id](mailto:atmaja_sri@umy.ac.id) (S.A.P. Rosyidi), [izzii@ukm.edu.my](mailto:izzii@ukm.edu.my) (Nur Izzi Md. Yusoff), [norfarahnadia@iiu.edu.my](mailto:norfarahnadia@iiu.edu.my) (N.N. Ismail), [razuhanafi@ukm.edu.my](mailto:razuhanafi@ukm.edu.my) (M.R.M. Yazid).

Peer review under responsibility of Ain Shams University.



Production and hosting by Elsevier

<https://doi.org/10.1016/j.asej.2020.05.006>

2090-4479/© 2020 THE AUTHORS. Published by Elsevier BV on behalf of Faculty of Engineering, Ain Shams University.

This is an open access article under the CC BY-NC-ND license (<http://creativecommons.org/licenses/by-nc-nd/4.0/>).

Please cite this article as: S. A. P. Rosyidi, N. I. M. Yusoff, N. N. Ismail et al., Integrated time–frequency wavelet analysis and impulse response filtering on SASW test for rigid pavement stiffness prediction, Ain Shams Engineering Journal, <https://doi.org/10.1016/j.asej.2020.05.006>

showed the promising potential of this technique in detecting rigid pavement profiles. Cho and Lin [5] employed the SASW method to conduct advanced study on multi-layered thin cement mortar slabs having a finite thickness. They found that the surface wave velocities of the experimental dispersion curves gradually increase with increasing age of the mortars. However, the values of surface wave velocity determined using the experimental compact dispersion curve are greater than those obtained based on the theoretical dispersion curve; this can be ascribed to the distinct boundary conditions and reflection at the boundaries. Kim et al. [6] combined two non-destructive testing, i.e. the Impact Echo (IE)–SASW method, to investigate concrete structures. The IE method was utilised for a detailed nondestructive evaluation of concrete while the SASW method was employed to establish the average P-wave velocity and for evaluating the status of concrete. Their studies were conducted on slab type concrete model specimens where different types of defects or boundaries were assigned at known locations.

This paper aims to highlight the research conducted to determine the stiffness of Portland cement concrete (PCC) slabs for each layer of rigid pavement structures by using the SASW method and to compare the equivalent moduli computed using the cylinder compression data obtained through the American Concrete Institute (ACI) formulation [7]. Advanced signal processing was also conducted in this study to examine the influence of boundary conditions and reflection in seismic measurement. This study also shows the potential of using the SASW method to non-destructively evaluate concrete structures, where masking procedure can be employed to deal with the influence of phase discontinuity in dispersion curve.

## 2. Description of methodologies

### 2.1. PCC slab properties

The tests for rigid pavements on PCC slabs were conducted on several slab prototypes (Fig. 1). Concrete class Type I cement with

maximum aggregates of 0.019 m were employed to fabricate the slabs. The concrete mixes for the PCC slab casts were specified for a 28-day compressive strength of 175 kg/cm<sup>2</sup> (17.14 MPa or 2,488.5 psi) and 225 kg/cm<sup>2</sup> (22.04 MPa or 3,200 psi). The cement–water ratio of the concrete 0.49 and the slump of the concrete is 0.035 m. The PCC slabs were placed over a compacted soil subgrade and have thickness of 200, 300, 400 and 450 mm.

### 2.2. Spectral analysis of surface wave method

#### 2.2.1. Field measurement

In reality, the majority of surface wave methods consist of three major steps: data acquisition, processing to extract the dispersion curve, and inversion [8–11]. Several researchers have studied the use of spherical mass or ball bearings to evaluate pavements by employing the SASW method [12–14]. Ball bearings (Fig. 2a) are dropped on pavement surface to produce a high frequency which is then used to generate *R* waves. Two receiving accelerometers were utilised to detect the waves at a 25 kHz sampling frequency (Fig. 2b). A spectrum analyzer was used to digitally analyze the signals and the results were displayed in selected spectrum functions, i.e. auto power spectrum and coherence function, to monitor the quality of the recorded signals. A typical equipment configuration is shown in Fig. 3. Various receiver configurations and source spacings are needed to sample varying depths of a rigid pavement profile. The measurement configuration for the SASW test in the present study is the midpoint receiver spacing [15]. The sample of the shallow layers of the profile were taken using small receiver spacings with a high frequency source while samples of deeper layers were taken employing greater receiver spacings with a set of smaller frequency sources. The space between the source and the near receiver is equivalent to the distance between receivers. This configuration is sufficient for minimizing near-field effect. The receiver spacings for the pair accelerometer were fixed at 5, 10 and 20 cm. High frequency sources such as a small ball bearing with a diameter of between 6.2 and 22 mm (Fig. 2a) were used to sample the PCC slabs.

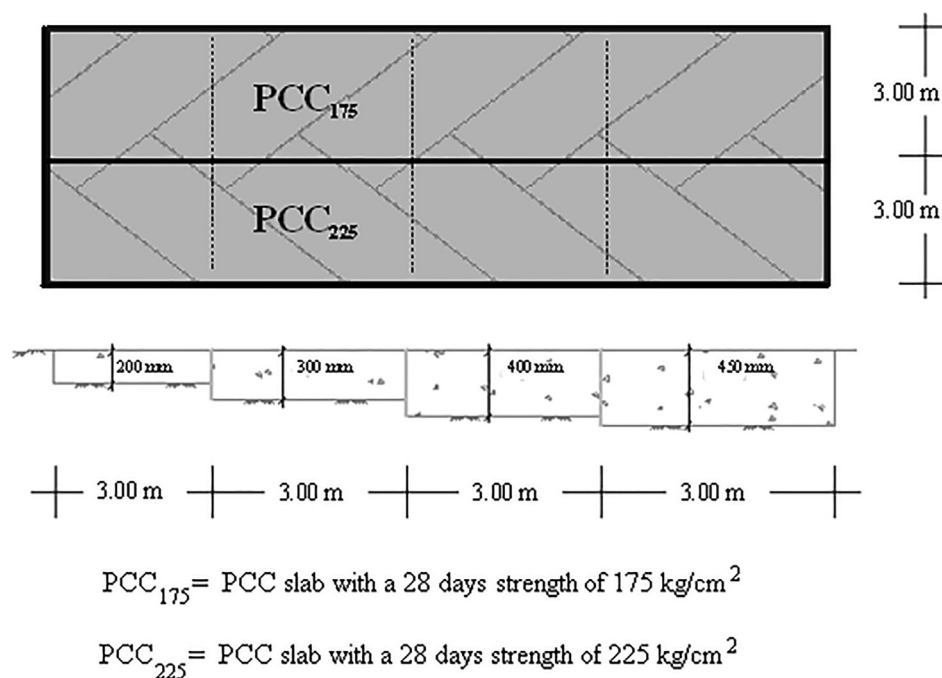


Fig. 1. Typical model of PCC slabs.

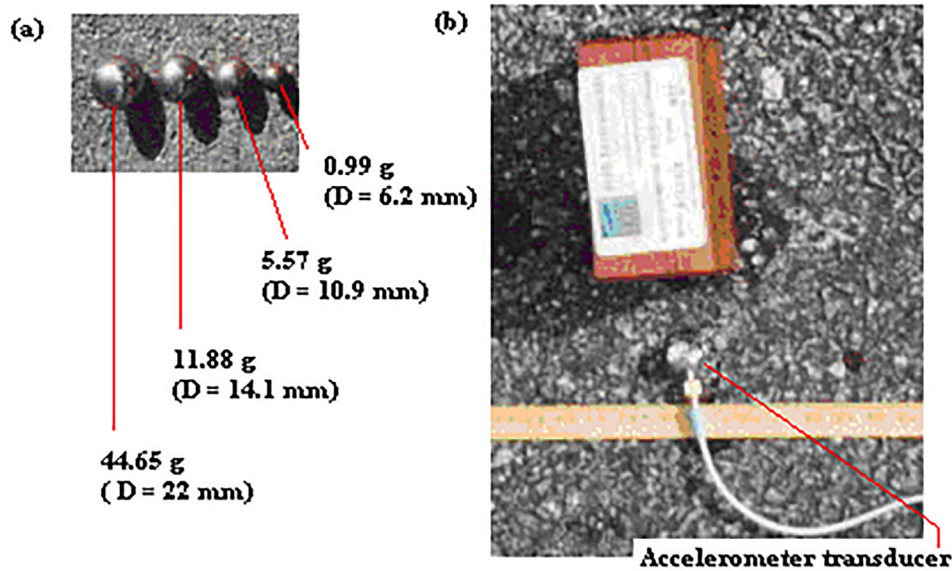


Fig. 2. High-frequency (a) sources and (b) sensor used in SASW measurement.

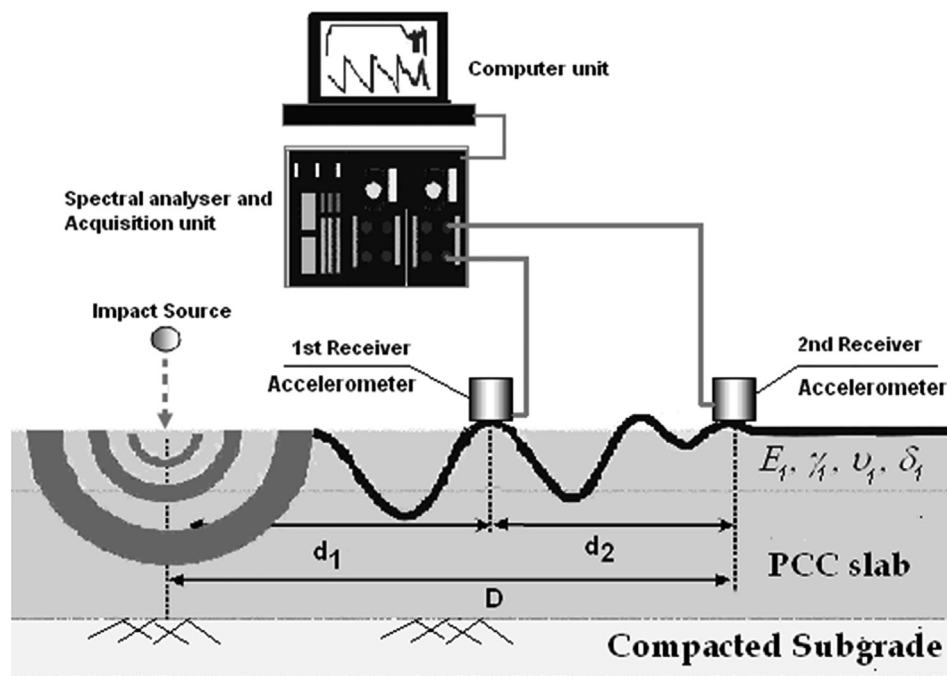


Fig. 3. Setup of SASW measurement.

### 2.2.2. Data analysis

Fig. 4 shows the general procedure used to analyze the data from SASW measurements taken in this study. The data analysis is divided into three steps up to the generation of the final profile of the rigid pavement model. In step 1, all signals from the collected data were converted into phase spectrum in the frequency domain. Ganji et al. [16] reported two advantages of transforming a wave field into a frequency domain, namely the wave propagation equation solution is readily available, and it is able to generate more information on propagation path [17]. In addition, analysis in the frequency domain is less ambiguous compared with that in the time domain [18]. The phase or transfer function spectrum is very crucial in identifying the relative phase shift between the two signals within the generated frequency range. Nevertheless, for an

intricate layered system with excessive difference in stiffness (i.e. rigid pavement), more than one wave group is being propagated as a result of wave refraction and reflection at the boundary of pavement layers. Thus, the transfer function spectrum is more complex and is influenced by the interface of varying wave groups. As a consequence, in-depth analysis of the wave groups registered during the propagation of waves on a complex layered system (step 2) has to be carried out in an effort to construct a precise phase dispersion curve of SASW measurement (Fig. 4).

Fig. 4 shows the two robust techniques, i.e. time-frequency (TF) based on continuous wavelet transform (CWT) and impulse response filtering (IRF), employed in this study. Wavelet analysis was utilised as a tool for analysing limited variations of power within a time series. Decomposition of a time series into time-

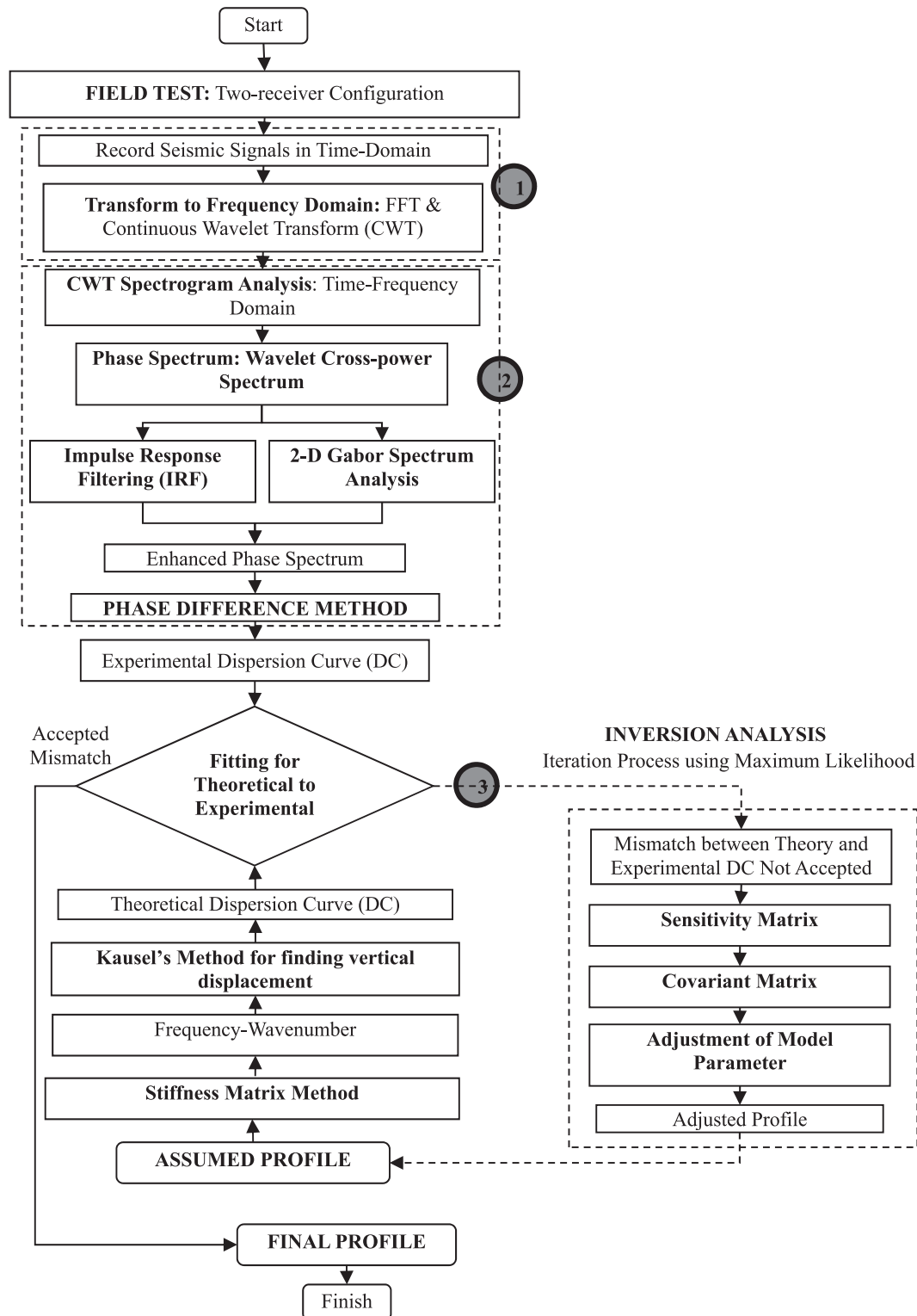


Fig. 4. Flow chart of the SASW Analysis used in this study.

frequency wavelet (TFW) spectrum allows for the determination of the dominant modes of variability and how these modes fluctuate with time. Alternatively, the CWT technique can be employed to localize the seismic frequency of interest in signal processing; in particular the non-stationary signal measured using the SASW method. The technique is even more important in seismic testing since CWT provides a redundant and detailed analysis of the signal description with respect to time and fre-

quency [19]. Many studies, such as those by Shokouhi and Gucunski [20], Kim and Park [21,22], Gucunski and Shokouhi [19], used wavelet transform to investigate the dispersion curve in the SASW method.

A wavelet is a function of  $\psi(t) \in L^2(\mathbb{R})$  with zero mean and is limited in both time and frequency. The dilation and translation of the wavelet,  $\psi(t)$ , makes it possible for it to be utilised for producing a wavelet families as:

$$\psi_{a,b}(t) = \frac{1}{\sqrt{|a|}} \psi\left(\frac{t-b}{a}\right), \text{ where } a > 0 \quad (1)$$

where  $a$  is a dilation parameter or scale and  $b$  is a translation parameter. It can be seen that if  $a > 1$ , the  $\psi_{a,b}(t)$  is a horizontally stretched and vertically compressed version of  $\psi(t)$ . The shape of wavelet that is suitable for signal analysis is dependent on seismic waveforms. However, there is no rule for determining the wavelet shape that is suitable for the best application. Gucunski and Shokouhi [19] pointed out that amongst all families of wavelet shapes, the Gaussian wavelet has been proven to be the most suitable for surface wave analysis.

CWT is the inner product of family wavelets, and a CWT of a seismic signal,  $f(t)$ , is a convolution between the signal and the function of wavelets  $\psi_{a,b}(t)$  which is shown as:

$$W_f(a, b) = \langle f(t), \psi_{a,b}(t) \rangle = \int_{-\infty}^{\infty} f(t) \frac{1}{\sqrt{|a|}} \bar{\psi}\left(\frac{t-b}{a}\right) dt \quad (2)$$

where  $\bar{\psi}$  is the complex conjugate of  $\psi$ , and  $W_f(u, s)$  is the time-scale map.

In this study, CWT was employed to convert the signals from the time domain to the frequency domain which display the wavelet spectrogram. Phase spectrum can then be generated from these wavelet spectrograms. For a layered system with strong stiffness contrast, a propagation of wave groups was detected. Hence, the phase difference spectrum is complicated and may result in misinterpretation when determining the correct values of the phase determined in the dispersion curve analysis. Impulse response and its filtering are more suitable for investigating wave groups in comparison to individual time signals since it focuses only on the response of the materials between receivers and is able to disregard the effect of source function in the time signals [23]. Fig. 5 presents the flow chart for the implementation of the CWT technique and the IRF of SASW method. The implementation procedure is as follows:

1. Choose the wavelet function and the set of scale,  $a = s$  (Eq. (1)), that will be employed in the transformation of the wavelet. Each wavelet function may affect time and frequency resolutions. The present study has chosen a Gaussian Derivative (GoD) wavelet function as the mother wavelet in CWT filtering. The filter design was used to extract the environmental noises and inappropriate wave groups influencing the wave signals.
2. Create a wavelet scalogram by executing the wavelet transform (Eq. (2)) utilizing the computed convolution of the seismic trace with a scaled wavelet dictionary. Calculation of wavelet scale was carried out as a fractional power of 2 by employing the formula proposed by Torrence and Compo [24]:

$$s_j = s_0 2^{j\delta_j}, j = 0, 1, \dots, J \quad (4)$$

$$J = \delta_j^{-1} \log_2 \left( \frac{N\delta_t}{s_0} \right) \quad (5)$$

where  $s_0$  is the smallest resolvable scale  $= 2\delta t$ ,  $\delta t$  is time spacing, and  $J$  is largest scale.

Transform the signal's scale dependent wavelet energy spectrum (scalogram) into a frequency dependent wavelet energy spectrogram to make a direct comparison with the Fourier energy spectrum.

3. Implement CWT filtration on the wavelet spectrogram by determining the time and frequency localization thresholds. In this study the CWT filtration was constructed using a simple truncation filter concept which only takes into account the passband

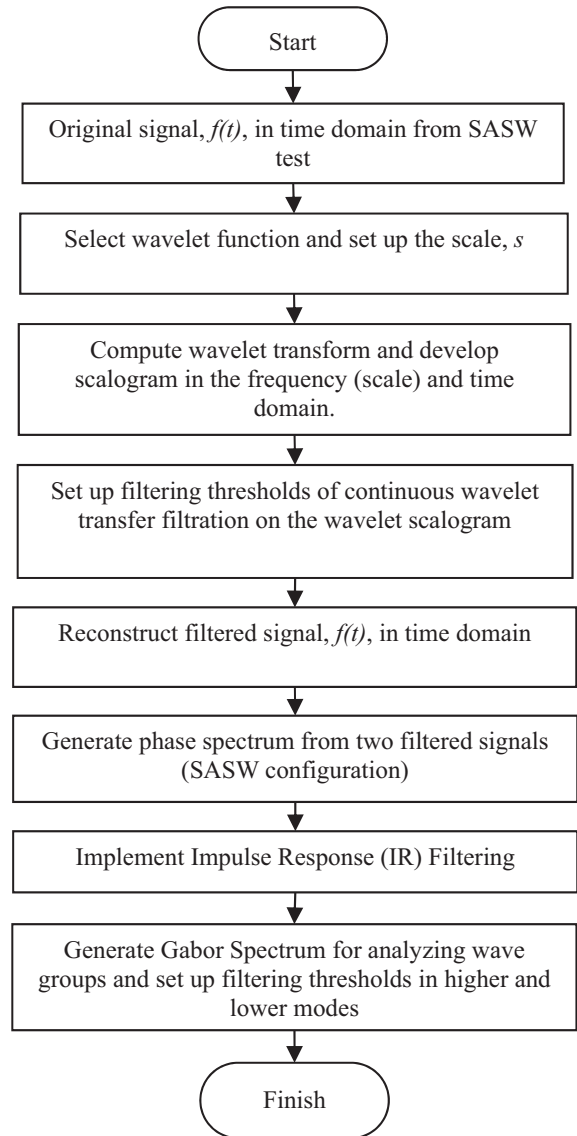


Fig. 5. Flow chart of CWT and IR filtering procedure.

and the stopband. Following this, the threshold values in the time and frequency domains were designated as the filter values between the passband and the stopband. This permits a straight filtering in all time, frequency, and spectral energy dimensions. The spectrum energy is zeroed out to eliminate the noisy or redundant signals; this completely removes the signals when rebuilding the time domain signal. Therefore, the relevant spectrum of signals will be passed when the spectrum energy is retained in the original value. Rosyidi and Taha suggested writing the CWT filtration design as follows [25]:

$$f(s) = \begin{cases} 0, & 1 \leq s \leq F_l \\ 1, & F_l \leq s \leq F_h \\ 0, & F_h \leq s \leq N \end{cases} \quad (6)$$

$$f(u) = \begin{cases} 0, & 1 \leq u \leq T_l \\ 1, & T_l \leq u \leq T_h \\ 0, & T_h \leq u \leq N \end{cases} \quad (7)$$

A value of 1 indicates that the spectrum energy is passed while a value of 0 is the filtration criteria when the spectrum energy is set to 0.

4. Calculate the phase difference using the reconstructed signals at each frequency to construct the phase spectrum for the experimental dispersion curve. The phase data is determined from the wavelet cross spectrum.

$$\varphi_n(s) = \arctan \left( \frac{\Im \{s^{-1} W_n^{XY}(s)\}}{\Re \{s^{-1} W_n^{XY}(s)\}} \right) \quad (8)$$

where  $W_n^{XY}(s) = W_n^X(s)W_n^{Y*}(s)$  = wavelet cross spectrum.

5. Perform impulse response filtering (IRF) from the phase spectrum. Joh [23] stated that impulse response can be obtained either through deconvolution of the signal in the time domain or through an inverse Fourier transform of the phase spectrum or transfer function. In this study, the impulse response was calculated using inverse Fourier transform since it is more practical and less time consuming.

6. Generate Gabor spectrogram for the impulse response.

7. Apply time window to the impulse response based on the Gabor spectrogram information. Time window can be obtained using two different approaches, i.e., the higher and the lower mode. The filter design proposed by Joh and Stokoe [26] consists of three bands: passband, transition band, and stopband (Fig. 6). The schematic design can be written as [26]:

$$f(n) = \begin{cases} 1, & 1 \leq n < P_l \\ \frac{1}{2} \cos \left( \frac{n-P_l}{L_l} \pi + 1 \right), & P_l \leq n < P_l + L_l \\ 0, & P_l + L_l < n < P_h, \text{ for higher mode} \\ \frac{1}{2} \cos \left( \frac{P_h+L_h-n}{L_h} \pi + 1 \right), & P_h \leq n < P_h + L_h \\ 1 & P_h + L_h < n \leq N \end{cases} \quad (9)$$

$$f(n) = \begin{cases} 1, & 1 \leq n < P_l \\ \frac{1}{2} \cos \left( \frac{P_l+L_l-n}{L_l} \pi + 1 \right), & P_l \leq n < P_l + L_l \\ 0, & P_l + L_l < n < P_h, \text{ for lower mode} \\ \frac{1}{2} \cos \left( \frac{n-P_h}{L_h} \pi + 1 \right), & P_h \leq n < P_h + L_h \\ 1 & P_h + L_h < n \leq N \end{cases} \quad (10)$$

where  $P_l$  and  $P_h$  are the initial points of the transition band;  $L_l$  and  $L_h$  are the cosine-tapered window length, and  $N$  is the total number of data point in the impulse response.

8. Calculate the modified phase spectrum of the filtered impulse response.

9. Unwrap the phase spectrum to obtain phase velocity. The phase (R) wave velocity coinciding to each wavelength is measured by unwrapping the phase angle data from the enhanced transfer function spectrum. The travel time between the receivers for each frequency is determined using Equation (11):

$$t(f) = \varphi(f)/360f \quad (11)$$

where  $f$  is frequency,  $t(f)$  is travel time at a given frequency, and  $\varphi(f)$  is phase difference in degrees at a given frequency.

10. Since the distance between receivers ( $d$ ) is a known parameter, the  $R$  of wave velocity,  $V_R$ , or the phase velocity at a given frequency can be determined as follows:

$$V_R = d/t(f) \quad (12)$$

and the coinciding wavelength for the  $R$  wave,  $L_R$ , can be expressed as:

$$L_R(f) = V_R(f)/f \quad (13)$$

Fig. 4 shows the inversion process carried out in step 3 to establish the shear wave velocity profile by means of experimental dispersion data. During the inversion process, the profile of a set of a homogeneous layer, such as rigid pavement surface, base, sub-base and subgrade layers, are assumed to extend to infinity in the horizontal direction. The last layer is typically assumed to be a homogeneous half-space. The present study employs an automated forward modeling analysis of the three-dimensional (3-D) dynamic stiffness matrix method [27] to obtain the best fitting between the theoretical and experimental dispersion curves. The model allows for the expansion of the displacement and stress (or traction) of the waves propagating on a horizontal surface by means of Fourier series in the circumferential direction as well as with respect to the cylindrical function (Bessel, Neuman or Hankel functions) in the radial direction. The axisymmetric loading requires only one Fourier series term (the 0 term), and the radial and vertical displacements ( $U$  and  $W$ ) are written as follows:

$$U(r) = qR \int_{k=0}^{\infty} \bar{u} J_1(kR) J_1(kr) dk \quad (14)$$

$$W(z) = qR \int_{k=0}^{\infty} \bar{w} J_1(kR_0) J_0(kr) dk \quad (15)$$

where  $J_0$  and  $J_1$  are the zero and the first order Bessel function,  $k$  is the wave number,  $r$  is radial distance from the source,  $R$  is the radius of the disk,  $q$  is the magnitude of the uniformly distributed load;  $\bar{u}$  and  $\bar{w}$  are the functions of  $k$  for a harmonic load at the surface with wavelength  $2\pi/k$ . According to Kausel and Peek [28] the displacements,  $\bar{u}$  and  $\bar{w}$ , in Eqs. (16) and (17), can be expressed as follows:

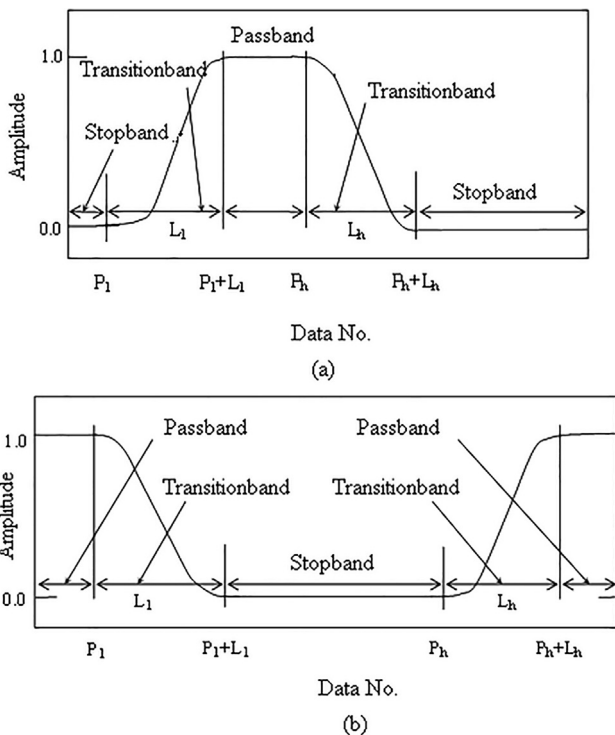


Fig. 6. Filtering of the (a) lower and (b) higher frequency modes.

$$\bar{u} = \sum_{i=1}^{2n+2} u_{i1} w_{i1} \frac{k}{k_i(k^2 - k_i^2)} \quad (16)$$

$$\bar{w} = \sum_{i=1}^{2n+2} w_{i1}^2 \frac{k}{k_i(k^2 - k_i^2)} \quad (17)$$

In an  $n$ -layer system over a half-space,  $u_{i1}$  and  $w_{i1}$  are the horizontal and vertical displacements on the surface in the  $i^{\text{th}}$  mode. This solution is especially useful when manipulating many layers, such as when a considerable variation of soil properties has to be determined. The theoretical dispersion curve constructed utilising the 3-D model is then coincided with the experimental dispersion curve based on lowest root mean square (RMS) error by using an optimization technique. The optimization technique used in this study drew on the maximum likelihood method proposed by Joh [23] and was carried out employing the WinSASW version 2.4 programme.

### 2.2.3. Calculation of concrete stiffness via shear wave velocity

The shear wave velocity parameter can be utilised to determine the dynamic shear moduli of pavement materials.

$$E = 2(\gamma/g)V_s^2(1 + \mu) \quad (18)$$

where  $E$  is dynamic elastic modulus,  $V_s$  is shear wave velocity,  $g$  is gravitational acceleration,  $\gamma$  is total unit weight of the material, and  $\mu$  is Poisson's ratio.

Nazarian and Stokoe [4] pointed out that a material's modulus obtained through seismic testing is similar to the highest at a strain of less than 0.001%. Within this range, a material's modulus is assumed to be constant.

### 2.3. Compressive strength testing in laboratory

A comparative test was carried out to evaluate concrete stiffness using standard cylinder (on 6 by 12-inch cylinder sample) compression tests (ASTM C 39) on the PCC slab samples. The compression tests were carried out for 3, 7, 10, 14, 17, 21 and 28 days after casting. The outcomes of the tests are shown in Table 1. The procedure used to calculate concrete stiffness is as follows: (a) several compression tests were conducted to establish the average compressive strength of the cylinders, and (b) the concrete slabs' dynamic stiffness obtained in these tests were then predicted using the ACI Committee 318 formulation [7], which is given as:

$$E_c = 33W_c^{1.5}f_c^{0.5} \quad (19)$$

$$E_d = 0.83E_c \quad (20)$$

where  $E_c$  is static elastic modulus of the concrete (in psi),  $E_d$  is dynamic elastic modulus of the concrete (in psi),  $W_c$  is unit weight of concrete (in pcf), and  $f_c$  is 28-day compressive strength (in psi).

**Table 1**  
Average values of compressive strength of PCC<sub>175</sub> and PCC<sub>225</sub> after curing.

Elapsed time (curing period) in days	Number of tests	Average compressive strength for PCC <sub>175</sub> (psi)	Average compressive strength for PCC <sub>225</sub> (psi)
3	3	1.28	2.07
7	3	2.30	3.19
10	3	2.32	3.56
14	3	2.39	3.64
17	3	2.44	3.76
21	3	2.50	3.90
28	3	2.63	4.11

## 3. Results and discussion

The tests conducted in the present study are particularly useful for quality control of PCC slabs. The tests include SASW to establish shear wave velocity and thickness; coring to determine pavement thickness; and laboratory compressive strength test as an alternative method for establishing the static stiffness of cement concrete. The values of phase and inverted shear wave velocities were used to calculate Young's or elastic modulus of PCC slabs on 3, 7, 10, 14, 17, 21 and 28 of curing days.

### 3.1. Experimental surface wave spectrum

An important step after the SASW data collection stage is the generation of a correct experimental dispersion curve. Fig. 7 shows an unfiltered experimental dispersion curve measured on a 40 cm-thick PCC<sub>175</sub> slab (i.e. PCC slab cast to have 175 kg/cm<sup>2</sup> of compressive strength) after a 17-day curing period. However, several wave modes and fluctuations were observed in the curves which are due to the reflection of shear, compression, and surface waves from the lateral and vertical boundaries of the PCC slab casts. Fig. 8 shows the time domain waveform of direct and reflected modes of the signals recorded by two accelerometer transducers on the PCC<sub>175</sub> slab surface after 17 days of curing. The direct surface waveform was shown as the first peak of wave amplitude and the amplitude subsequently decreased with time. The reflected waveform was recognized from several peaks of the recorded signal following the direct surface waveform. However, the wave groups of the direct surface waves cannot be easily isolated and separated from the direct body waves and their reflected waves in the time domain of the recorded signal. However, it can be easily observed in the Fourier spectrum of these direct and reflected waveforms by using the frequency response peak. Fig. 9 shows that the result of FFT analysis on the time domain of the recorded signals yields the auto spectrum function for each receiver. The group of direct and reflected waves produced varying frequency response peaks. The primary wave groups were found within the high frequency range of 9–15 kHz and 11–14 kHz for channels 1 and 2, respectively. The interference of the different wave groups might generate an uneven or vague phase or transfer function spectrum (Fig. 10). Thus, the wavelet analysis time–frequency (TF) and interactive signal processing of an impulse response filtering (IRF) recommended by Joh [23] were performed. This reduced the fluctuation in the dispersion curve, as illustrated in Fig. 7.

The present study utilised the mother wavelet of the Gaussian Derivative. The real component of the Gaussian Derivative wavelet in the time and frequency domains is expressed as the following:

$$\psi_0(t) = \frac{(-1)^{m+1}}{\sqrt{\Gamma(m + (1/2))}} \frac{d^m}{dt^m} \left( e^{-t^2/2} \right) \quad (21)$$

$$\hat{\psi}_0(s\omega) = -\frac{i^m}{\sqrt{\Gamma(m + (1/2))}} (s\omega)^m \left( e^{-(s\omega)^2/2} \right) \quad (22)$$

where  $m$  is the wave number.

The generation of complex wavelet is done via the addition of a Heaviside function to the frequency domain. This wavelet decays with the square root of the gamma function. The derivative order of the Gaussian Derivative can be changed to obtain the waveform with the optimal resolution. The Gaussian's second order exponential decay utilised in the time resolution plot produced an exceptional time localization.

This is followed by employing the time–frequency (TF) analysis of CWT in order to overcome the difficulty of identifying the spectral characteristics of non-stationary signals registered by the two receivers. Fig. 11 shows the standard CWT spectrogram for the

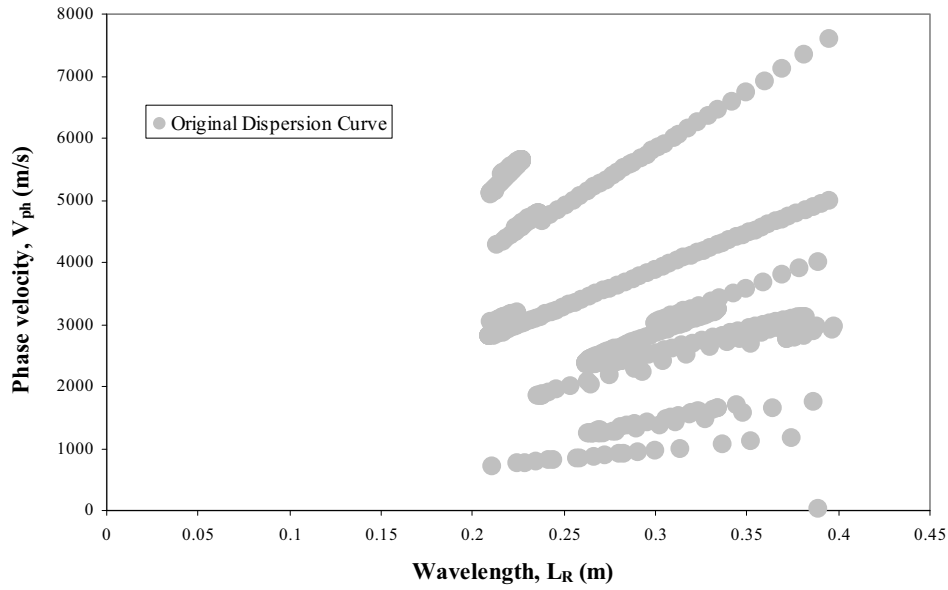


Fig. 7. Original experimental dispersion curve measured on a 40 cm PCC<sub>175</sub> slab after 17 days of curing.

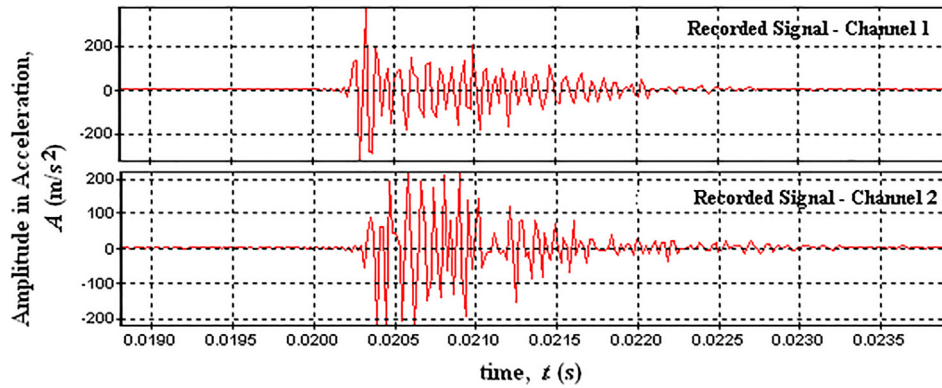


Fig. 8. Time signals of a 40 cm PCC<sub>175</sub> slab at 20 cm receiver spacing after 17 days of curing.

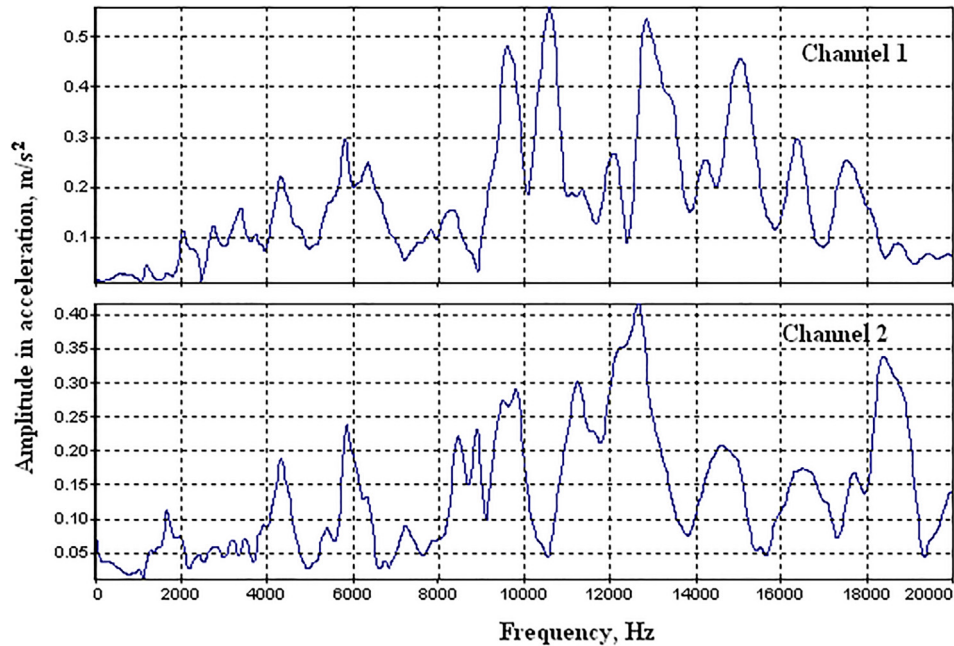


Fig. 9. Auto power spectrum for receivers 1 and 2 from measurements on a 40 cm PCC<sub>175</sub> slab at 20 cm receiver spacing after 17 days of curing.

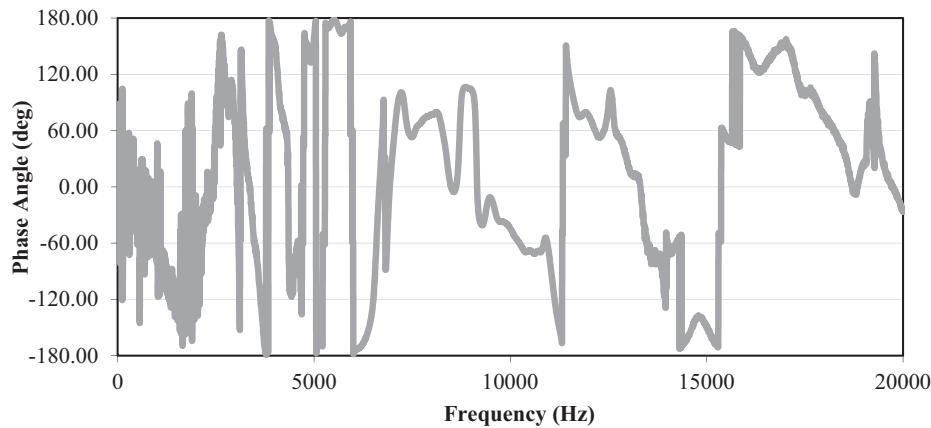


Fig. 10. Original phase spectrum of a 40 cm PCC<sub>175</sub> slab at 20 cm receiver spacing after 17 days of curing.

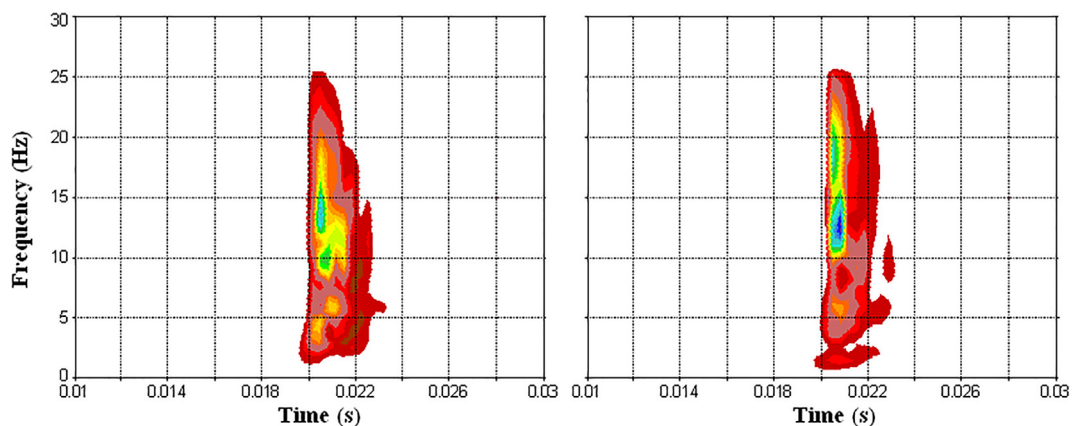


Fig. 11. TF spectrum for recorded signals at receivers 1 and 2 from measurement on a 40 cm-thick PCC<sub>175</sub> slab at 20 cm receiver spacing after 17 days of curing.

received signals with an enhanced time–frequency resolution. The TF of Gaussian Derivative wavelet produced a good resolution at high frequency and is useful for detecting the frequency bandwidth of wave groups by utilizing different derivation orders of this wavelet.

Fig. 11 shows that there are a number of energy events at varying frequency bands which could cause interference at low and higher mode of seismic signals. These energy events of the wave groups are within 0.019–0.022 s of arrival time (received by the accelerometers). It can be seen that the dominant energy event occurred between 9 and 20 kHz in both CWT spectrograms. Within this range, two other peak events have been detected and they have been identified as direct surface wave and interference of reflected body waves. The first event occurred at high frequency in the 9–13 kHz range (channel 1) and 10–13 kHz range (channel 2) and has been identified as the direct surface wave propagation. The energy of the reflected body waves was first captured by the receivers. It can be found in the higher frequency range (13–18 and 15–21 kHz in channels 1 and 2, respectively). The other wave group was an earlier arrival which appeared in the lower frequency range below approximately 7 kHz. This group can be classified as the direct primary and secondary body wave which arrived in the earlier period of signal recording, which is also known as the near-field effect.

The apparent spectrum of TF plot based on the integrated-power of wave magnitude is shown in Fig. 12. The highest peak curve on the integrated-power amplitude versus frequency plot shows the dominant energy recorded from the measurement and

it represents the energy from the surface wave and the interference of body wave. Therefore, the continuous Gaussian Derivative wavelet transform is able to clearly show that the superposition of energy from several wave groups occurred in the time–frequency spectrum of the seismic signal recorded from SASW measurement. It was also observed that, in pavement models with strong stiffness contrast, the interference of body waves is still included in the dynamic response on material. It is important to maintain the interference of body wave in the phase spectrum since valuable information on subsurface stratification and stiffness is contained in the phase spectrum. In addition, the stiffness matrix method [27,28], which was used in the inversion analysis of this study, utilised the body-wave interference.

In order to extract only the relevant portion of time signals which correspond to a specific group, the Wavelet-IRF technique was then used. Impulse response is capable of showing the response of materials between the two receivers used in the SASW measurement. Fig. 13 shows the impulse response obtained from the first integration of the phase spectrum. The Wavelet-IRF filters used to enhance a noisy phase spectrum should be designed to include as much time signal as possible and should be able to minimize the phase shift caused by filtering. In order to show the information of Wavelet-IRF parameter which separate the lower and higher modes, the Gabor spectrogram was generated, as shown in Fig. 14. The Gabor spectrogram represents time signal as a linear combination of time–frequency-shifted Gaussian function, which is a good tool for wave groups investigation in impulse response. The time–frequency plot concept of Gabor spectrogram is similar with

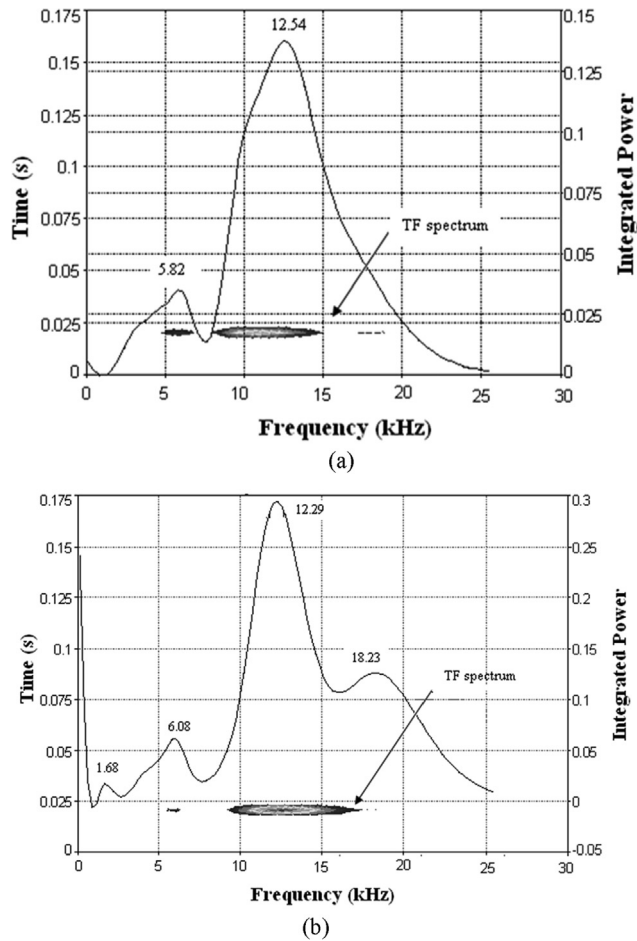


Fig. 12. TF spectrum and integrated-power versus frequency plot of recorded signals at receivers (a) 1, and (b) 2 from time signals (Fig. 7) for detecting the wave groups recorded in each receiver.

TF-CWT, as mentioned earlier. Fig. 14 shows several distinct wave groups. One is an earlier arriving group mode in the 17 to 20 kHz frequency range which was designated as the interference of body

wave. It appeared at arrival time less than 1.6 ms. The other wave group appeared in the 10–13 kHz frequency range, which are the direct surface waves since they were the next wave to be detected after the reflected body waves. A later arrival of wave groups was in the lower frequency range (below 2.3 kHz) and for a duration of up to 0.4 ms. The lower frequency group yields lower velocity waves compared to the waves at higher frequency. In this study, the later arrival of wave groups and lower frequency is called a lower mode and the earlier arrival is called the high mode. The filtering criteria was implemented for the earlier part of the impulse response (high frequency mode in the slab). This was identified in the 0–2.88  $\mu$ s range (Fig. 13) and the signals outside of this range were filtered out. The enhanced phase spectrum function was then regenerated (Fig. 15). After unwrapping the enhanced phase spectrum, an enhanced experimental dispersion curve was plotted.

Fig. 16 shows the experimental dispersion curve measured after a 17-day curing of PCC slabs. An important aspect of Fig. 15 is that the enhanced experimental dispersion curves with wavelength less than slab thickness of 0.2–0.4 m are almost constant, which indicate that only cured concrete was sampled. Fig. 16 shows the corresponding shear wave velocity profile obtained by inverting the experimental dispersion curve. The inversion analysis was carried out using the 3-D stiffness matrix method with the maximum likelihood optimization technique. The uncertainty factor of phase velocity data from experimental dispersion curve was assumed to be 0.05 while for model parameters of shear wave velocity and thickness they were assumed to be 0.05 and 0.15, respectively. These factors represent the standard deviation (SD) implemented in the analysis. Fig. 17 presents the shear wave velocity profile with the lower and upper velocity boundary calculated from the SD. Three layers of observed PCC slabs were detected in the profiles. The velocity differences in these layers were caused by different layering during model (physical) construction. The average value of the shear wave velocity obtained via SASW inversion of PCC<sub>175</sub> after 17 days of curing is 2061.71 m/s. By using this value, the Young's modulus of PCC slab can be easily obtained using Eq. (7).

### 3.2. Variation of surface wave velocity and dynamic stiffness with time

A fundamental assumption in the utilisation of in situ surface wave technique to determine the engineering characteristics of

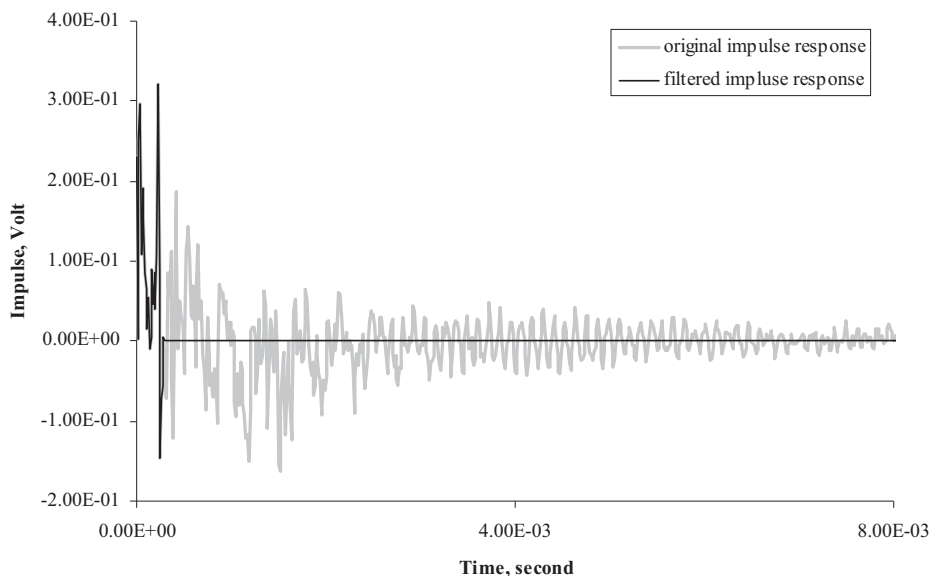


Fig. 13. Impulse response filtering of phase spectrum function obtained from Fig. 9.

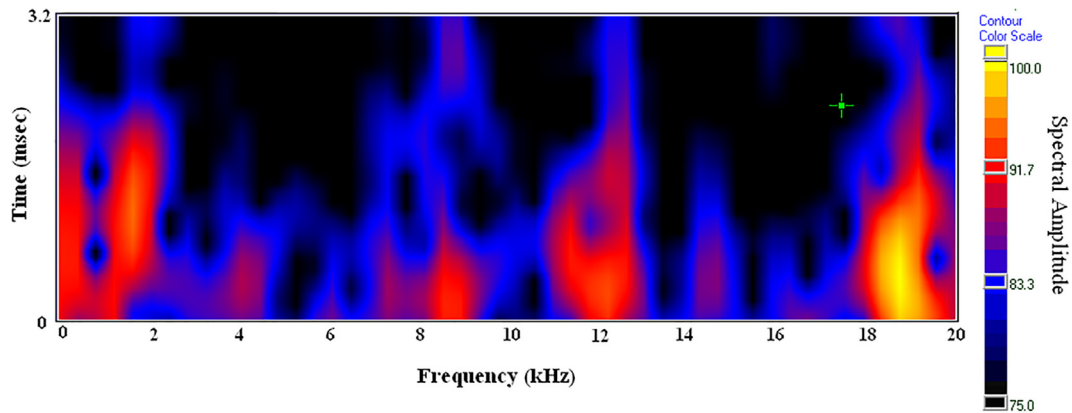


Fig. 14. Gabor spectrum of a 40 cm PCC<sub>175</sub> slab at 20 cm receiver spacing after 17 days of curing.

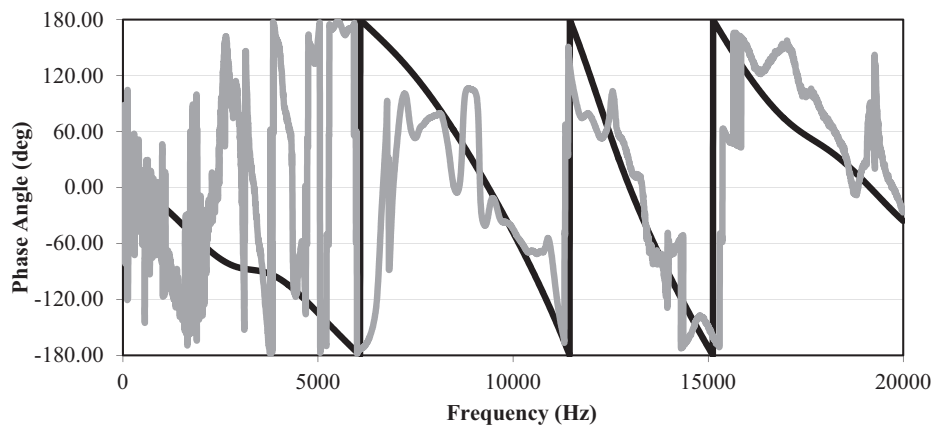


Fig. 15. Original and enhanced phase spectrum of a 40 cm PCC<sub>175</sub> slab at 20 cm receiver spacing after 17 days of curing.

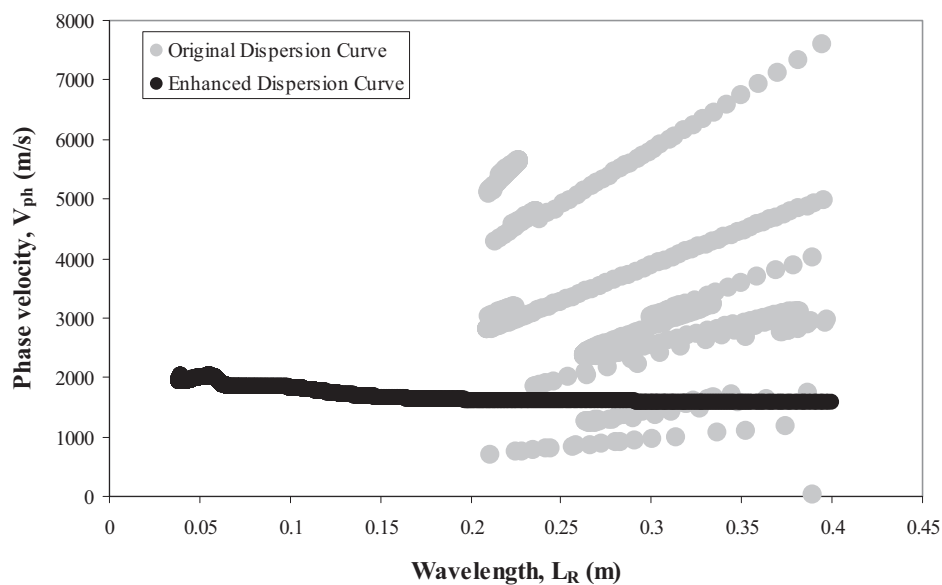


Fig. 16. Original and enhanced experimental dispersion curve measured on a 40 cm PCC<sub>175</sub> slab after 17 days of curing.

cured PCC slabs is that the changes observed in the  $R$  wave velocity and shear wave velocity coinciding with the dynamic stiffness of material during curing are direct indicators of the curing process. In order to acquire the data for proving the above hypothesis, sev-

eral SASW tests were conducted on the PCC slabs at each compressive strength (PCC<sub>175</sub> and PCC<sub>225</sub>) after the slabs were poured and finished, and the tests were continued throughout the curing time of 3, 7, 10, 14, 21 and 28 days.

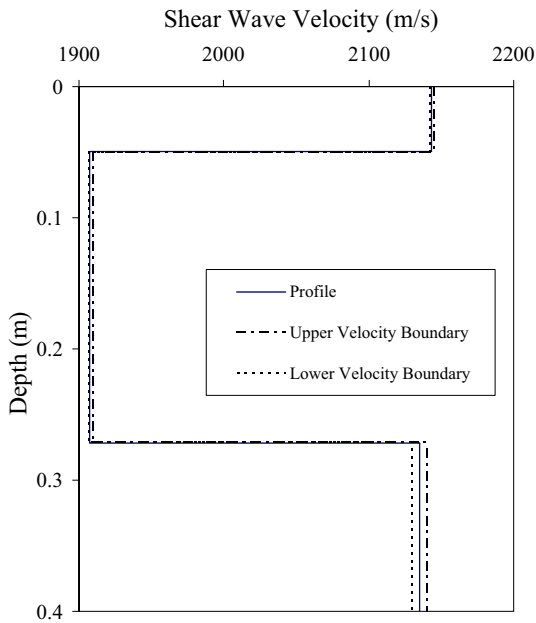


Fig. 17. Shear wave velocity profile of PCC<sub>175</sub> after 17 days of curing.

The increase in *R* wave velocity with time for each observed PCC slabs is shown in Fig. 18. The wave velocity increased rapidly initially and then began to level off after about 28 days. Intuitively, this behavior imitates the expected curing process. This result shows that surface wave velocity is a promising parameter for stiffness control in the curing process of the concrete slabs. Table 2 pre-

sents the outcomes of the student-*t* statistics test which was performed on the *R* wave data to verify the congruity of the results in testing repetitions. The calculated *t* values do not exceed the tabulated values with a level of significance of  $\alpha = 0.05$ . This means that the measured *R* wave data for both PCC slabs are consistent and significantly homogenous in each elapsed time observation.

The value of Young's moduli was calculated based on inverted-shear wave velocity as explained earlier. The unit weight values of concrete in each PCC slabs were measured at each elapsed time of the curing process. Assumption of the different values of Poisson's ratio of the concrete during the curing process was based on the values obtained by Rix et al. [29]. Fig. 19 presents the measured values of the Young's modulus for concrete PCC slabs at various elapsed time of the curing process.

### 3.3. Comparison of seismic stiffness with concrete stiffness from the ACI formulation

The stiffness dynamic concrete in the cylinder compression test were calculated using the ACI formulation. Fig. 20 shows that there is a good agreement between the concrete moduli values obtained through the SASW test and the values predicted from the results of the cylinder compression test by using the ACI formulation which give a coefficient of determination ( $R^2$ ) of 0.91. In general, the value of concrete moduli measured via the SASW test is slightly higher than the value obtained from the cylinder compression test. One possible reason for this is that seismic measurements determine Young's modulus at a very small strain, i.e. at approximately less than 0.001%, whereas the ACI formulation predicted the values of Young's elastic modulus at higher strain levels. Another possible reason for the difference between the two measurements is the dif-

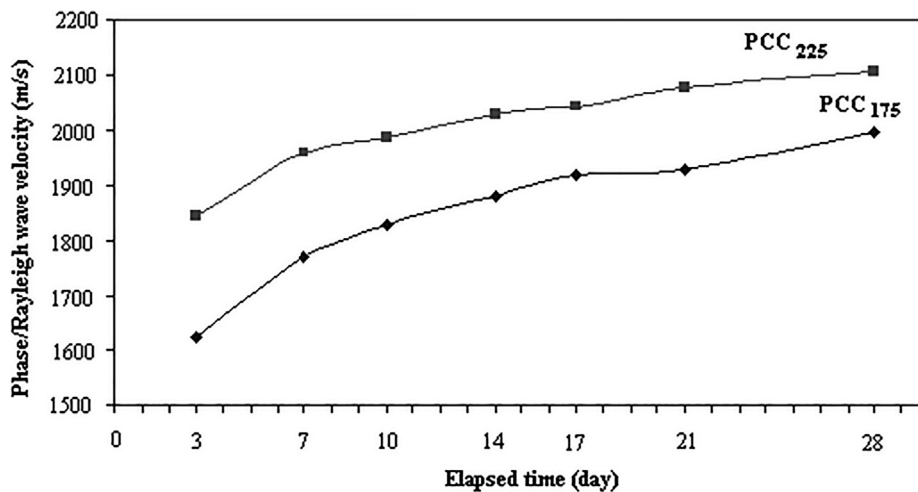


Fig. 18. Change in phase velocity with time for both PCC slabs.

Table 2  
Average values of phase wave velocity of PCC<sub>175</sub> and PCC<sub>225</sub> at curing time.

Elapsed time (day)	N	PCC <sub>175</sub>				PCC <sub>225</sub>			
		Mean (m/s)	Std. Deviation (m/s)	Std. Error (m/s)	<i>t</i> <sub>value</sub>	Mean (m/s)	Std. Deviation (m/s)	Std. Error (m/s)	<i>t</i> <sub>value</sub>
3	16	1624.40	22.88	11.44	1.206	1843.12	21.22	10.61	1.503
7	16	1768.03	86.23	43.11	-2.223	1958.38	20.56	10.28	-1.096
10	16	1828.51	62.28	31.14	-1.268	1987.52	87.07	43.53	-2.290
14	16	1880.90	72.66	36.33	-0.340	2029.35	82.26	41.13	-1.702
21	16	1917.58	32.53	16.26	1.902	2043.58	77.10	38.55	-1.733
28	16	1927.00	62.65	31.82	0.728	2076.77	47.14	23.57	-2.520

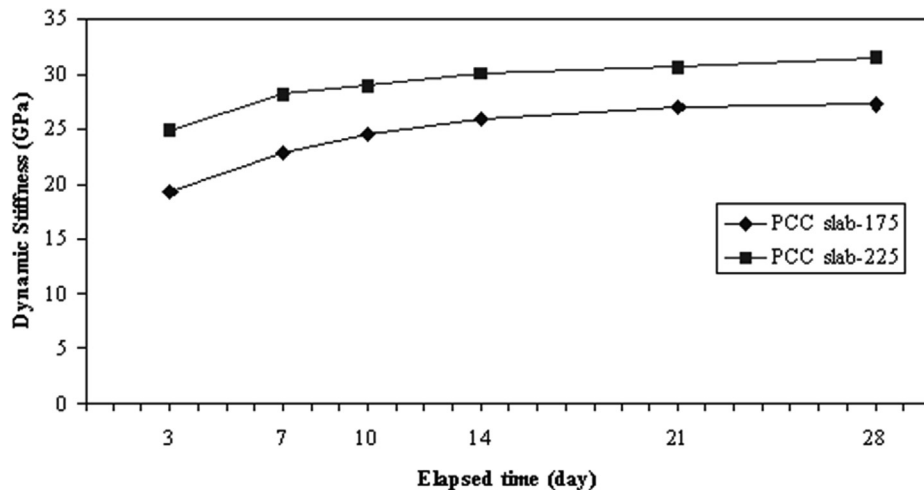


Fig. 19. Change in dynamic stiffness with time for both PCC slabs.

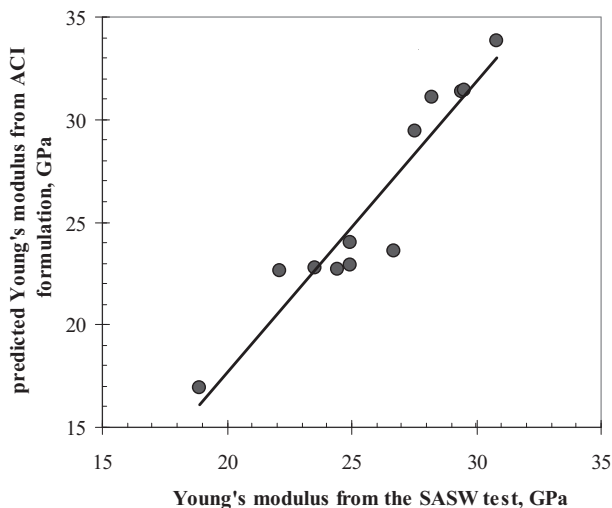


Fig. 20. Comparison of Young's modulus obtained from the SASW test and the modulus predicted from the ACI formulation using the cylinder compression test.

ferent curing rate of the concrete in the slabs and the concrete in the cylinder samples.

Thus, the usefulness of SASW for predicting elastic modulus has been established. SASW could also be used to detect weak spots in a pavement profile (both longitudinal and vertical). This procedure could provide a quick and efficient analysis of concrete slabs due to its efficiency in addition to the benefit of not requiring the conventional destructive sampling. This highlights the advantage of using in situ seismic measurement to evaluate the properties of concrete in real condition.

#### 4. Conclusion

The present study predicts the concrete stiffness of two PCC slabs by performing SASW test. An improved spectrum analysis in the SASW method which employs continuous wavelet spectrogram analysis was also proposed. The denoising and reconstruction technique for the response spectrum from surface wave propagation by utilizing time–frequency spectrogram analysis of continuous wavelet transforms and impulse response filtering (IRF) technique was also presented. The 2-D wavelet spectrogram is able to precisely establish the relevant different events in the seismic

surface waves and noisy signals. The threshold for CWT and Impulse Response (IR) filtration was derived from the generated spectrogram. In consequence, the reconstruction of the denoised signals of the seismic surface waves can be carried out utilizing inverse wavelet transform which takes into account the thresholds of the relevant spectrum. Results showed that SASW is very sensitive and can be successfully used to determine the  $R$  velocity parameter of slabs. By obtaining the inverse of  $R$  wave velocity using the dynamic stiffness matrix method, the shear wave velocity corresponding to the Young's modulus of PCC slabs is obtained. The  $R$  velocity parameter is also useful for detecting the degree of stiffness change in the observed PCC slabs during the curing process. The in situ measurement using the SASW method offer a potentially useful alternative to conventional cylinder compression test for determining the dynamic stiffness characteristics of PCC slabs. There is a good congruence between the Young's modulus determined using the SASW and ACI methods. Thus, SASW is very suitable for carrying out in situ measurement of the Young's modulus profile of the entire rigid pavement system.

#### Acknowledgements

The authors would like to extend their sincere appreciation to the Faculty of Engineering, Muhammadiyah University of Yogyakarta (UMY), the Ministry of Research, Technology and Higher Education, Republic of Indonesia and Universiti Kebangsaan Malaysia (GUP-2018-094) for supporting this research program. The authors also would like to thank Prof. Sung Ho-Joh, Mr. Wendy Artyanto, Mr. Sigit Sunarjati, Mr. Wawan Kurniawan and Mr. Eko Rahadi for their assistance during the field and data processing work.

#### References

- [1] Kirlangic AS, Cascante G, Polak MA. Assessment of concrete beams with irregular defects using surface waves. *ACI Mater J* 2016;113(1):73–81.
- [2] Nazarian S, Stokoe KHII. In-situ shear wave velocity from spectral analysis of surface waves. In: 8th World Conference on Earthquake Engineering, vol. 3; 1984, p. 31–8.
- [3] Jones RB. In-situ measurement of the dynamic properties of soil by vibration methods. *Geotechnique* 1958;8:1–21.
- [4] Nazarian S, Stokoe KHII. In situ determination of elastic moduli of pavement systems by Spectral-Analysis-of-Surface-Wave method (theoretical aspects). Austin: The University of Texas at Austin. Research Report 437-2, Center of Transportation Research; 1986.
- [5] Cho YS, Lin F-B. Spectral analysis of surface wave response of multi-layer thin cement mortar slab structures with finite thickness. *NDT&E Int* 2001;34:115–22.

- [6] Kim DS, Seo SW, Lee KM. IE-SASW method for nondestructive evaluation of concrete structure. *NDT&E Int* 2006;39:143–54.
- [7] ACI Committee 318, Building Code Requirements for Reinforced Concrete. Detroit: American Concrete Institute; 1995.
- [8] Arai H, Tokimatsu K. Velocity profiling by joint inversion of microtremor dispersion curve and horizontal-to-vertical (H/V) spectrum. *Bull Seismol Soc Am* 2005;95(5):1766–88.
- [9] Ikeda T, Matsuoka T, Tsuji T, Hayashi K. Multimode inversion with amplitude response of surface waves in the spatial autocorrelation method. *Geophys J Int* 2012;190:541–52.
- [10] Foti S, Lai C, Rix G, Strobbia C. Surface wave methods for near-surface site characterization. Boca Raton, Florida: CRC Press, Taylor & Francis Group; 2014.
- [11] Garofalo F, Foti S, Hollender F, Bard PY, Cornou C, Cox BR, et al. InterPACIFIC project: Comparison of invasive and non-invasive methods for seismic site characterization. Part I: Intra-comparison of surface wave methods. *Soil Dyn Earthq Eng* 2016;82:222–40.
- [12] Kumar J, Hazra S. SASW testing of asphaltic pavement by dropping steel balls. *Int J Geotech Eng* 2014;8(1):34–45.
- [13] Kumar Jyant, Hazra Sutapa. Effect of input source energy on SASW evaluation of cement concrete pavement. *J Mater Civ Eng* 2014;26(6):04014013. doi: [https://doi.org/10.1061/\(ASCE\)MT.1943-5533.0000827](https://doi.org/10.1061/(ASCE)MT.1943-5533.0000827).
- [14] Kumar J, Naskar T. Effects of site stiffness and source to receiver distance on surface wave tests' results. *Soil Dyn Earthq Eng J* 2015;77(1):71–82.
- [15] Heisey JS, Stokoe KHII, Meyer AH. Moduli of pavement systems from Spectral Analysis of Surface Waves. *J Transp Res Board* 1982;852:22–31.
- [16] Ganji V, Gucunski N, Nazarian S. Automated inversion procedure for spectral analysis of surface waves. *J Geotech Geoenviron Eng* 1998;124(8):757–70.
- [17] Bath M. Spectral analysis in geophysics. Amsterdam: Elsevier Scientific Publication Co.; 1974.
- [18] Nolet G, Panza GF. Array analysis of seismic surface waves: limits and possibilities. *Pageoph* 1976;114:775–90.
- [19] Gucunski N, Shokouhi P. Wavelet transform in surface wave analysis. In: *GSP 134 Soil Dynamics Symposium in Honor of Professor Richard D. Woods*. ASCE; 2015.
- [20] Shokouhi P, Gucunski N. Application of wavelet transform in detection of shallow cavities by surface waves. In: *Proceeding of SAGEEP, EEGS, San Antonio, TX*; 2003.
- [21] Kim D, Park HC. Evaluation of dispersion phase velocities using harmonic wavelet transform. *NDT&R Int* 2001;34:457–67.
- [22] Kim D, Park HC. Determination of dispersion phase velocities for SASW method using harmonic wavelet transform. *Soil Dyn Earthquake Eng* 2002;22:675–84.
- [23] Joh SH. Advances in data interpretation technique for spectral analysis-of-surface-waves (SASW) measurements Dissertation (PhD). The University of Texas at Austin; 1996.
- [24] Torrence Christopher, Compo Gilbert P. A practical guide to wavelet analysis. *Bull Am Meteor Soc* 1998;79(1):61–78. doi: [https://doi.org/10.1175/1520-0477\(1998\)079<0061:APGTWA>2.0.CO;2](https://doi.org/10.1175/1520-0477(1998)079<0061:APGTWA>2.0.CO;2).
- [25] Rosyidi SAP, Taha MR. Wavelet spectrogram analysis of surface wave technique for dynamic soil properties measurement on soft marine clay site. In: Kanao Masaki, editor. *Seismic waves - research and analysis*. InTech; 2012. doi: <https://doi.org/10.5772/27530>.
- [26] Joh SH, Stokoe KHII. Impulse response filtration technique for the determination of phase velocities from SASW measurements. *J Korean Geotech Soc* 1997;13:111–21.
- [27] Kausel E, Rössset JM. Stiffness matrices for layered soils. *Bull Seismol Soc Am* 1981;71(6):1743–61.
- [28] Kausel E, Peek R. Dynamic loads in the interior of a layered stratum: an explicit solution. *Bull Seismol Soc Am* 1982;72(5):1459–81.
- [29] Rix GJ, Bay JA, Stokoe KHII. Assessing in situ stiffness of curing Portland cement concrete with seismic tests. *J Transp Res Board* 1990;1284:8–15.



**Dr. Sri Atmaja P. Rosyidi** currently is an Associate Professor in the Department of Civil Engineering, Universitas Muhammadiyah Yogyakarta, Indonesia. His research interests are mainly in the area of pavement, railway and transportation engineering.



**Ir. Dr. Nur Izz Md. Yusoff** currently is an Associate Professor in the Department of Civil Engineering, Universiti Kebangsaan Malaysia, Malaysia. His research interests are mainly in the area of pavement engineering and pavement materials.



**Dr. Norfarah Nadia Ismail** currently is an Assistant Professor in the Department of Civil Engineering, International Islamic University Malaysia, Malaysia. Her research interests are mainly in the area of pavement and geotechnical engineering.



**Ts. Ir. Dr. Muhamad Razuhanafi Mat Yazid** currently is a Senior Lecturer in the Department of Civil Engineering, Universiti Kebangsaan Malaysia, Malaysia. His research interests are mainly in the area of pavement and transportation engineering.